The International Journal of Advanced Manufacturing Technology (2020) 109:1409–1418
https://doi.org/10.1007/s00170-020-05751-7

ORIGINAL ARTICLE

Detection of tool breakage during milling process through acoustic emission

Shixu Sun[1] · Xiaofeng Hu[1] · Wenjuan Zhang[2]

Received: 17 January 2020 / Accepted: 8 July 2020 / Published online: 16 July 2020

Abstract

Catastrophic tool failure (CTF) in milling process can cause damage to the product's machined surface and the machine tools, leading to huge financial losses. It is therefore critical to detect CTF in advance and promptly respond to it. Because of the safety and quality requirements imposed in practice, there are far fewer failure samples than normal samples, and this disequilibrium makes it difficult to detect failures. The aim of this study is to develop a new, easy, and practical automatic system for tool breakage detection using the acoustic emission (AE) technique. Components of AE raw data are analysed to locate the moments of tool breakages and to screen the corresponding AE feature samples. A support vector machine-based cost-sensitive breakage detection model is established and optimized. The proposed model is applied and validated by experiments conducted on a factory's milling machine. The model achieves an accuracy of 91.18% in the detection of breakages. The results show the practicability and validity of the proposed method.

Keywords Tool breakage · Catastrophic tool failure · Acoustic emission · Support vector machine · Short-time Fourier transform

1 Introduction

The turbine generator is one of the most important pieces of equipment in the power industry. As a core component of the generator, the generator rotor is high-value-added and complicated. It is manufactured through a milling process with a high flexibility and high removal rate. A high level of accuracy and surface quality can be achieved using hard tools; however, this increases the risk of unexpected catastrophic tool failure (CTF) [1, 2]. Without a tool breakage detection system, CTF during the cutting procedure can cause damage to the machined surface of the product and the machine tools, causing huge financial losses. Hence, it is crucial to build an automatic monitoring system to detect tool breakages and prevent the occurrence of CTF during the milling operation.

Monitoring techniques of machining operations are traditionally categorized into either direct measurement methods or indirect measurement methods. Compared with direct measurement methods, indirect measurement methods have the advantage of real-time detection. They also have few influence on the machining process, making them more suitable for practical applications [3, 4]. Various signals, such as acoustic emission (AE) [5–7], acceleration [8, 9], cutting force [10, 11], and power [12] corresponding to tool condition, quality of machining, and defects in the workpiece, have been researched. Studies have well examined that the sensing signals during the cutting process provide one of the most effective means to detect tool breakages [13, 14]. Rehorn et al. [15] and Zhou et al. [4] reviewed these various methods that have been adopted to monitor tool condition, indicating that AE can provide marked and rapid responses to the changes in a tool's condition. Furthermore, it is easily recorded and unaffected by vibrations and noises since the frequency of the AE signal is much higher than the frequency of that [16].

Many techniques can be used to detect tool breakages, such as support vector machines (SVMs) [17–19], artificial neural networks [20], Bayesian networks [21], and hidden Markov models [22]. Most of these methods require a great number of

✉ Xiaofeng Hu
wshxf@sjtu.edu.cn

Shixu Sun
sunshixu13@sjtu.edu.cn

[1] School of Mechanical Engineering, Shanghai Jiao Tong University, Shanghai 200240, China

[2] Warwick Business School, University of Warwick, Coventry CV47AL, UK

labelled samples under constant conditions to establish the model. However, SVMs can effectively deal with small training data sets and can produce a higher classification accuracy than other traditional methods [23, 24]. In terms of the manufacturing process of a generator rotor, labelled samples, particularly samples of broken tools, are rare. The sample size is too small for most methods except SVMs. Additionally, there are far fewer broken tool samples than normal samples, and this disequilibrium makes it more difficult to recognize the minority class (the broken tool samples) than the majority class (the normal samples) [25, 26]. To deal with this imbalance, techniques such as sampling methods [27], cost-sensitive methods [28, 29], and other methods have been proposed. Various empirical studies have shown that cost-sensitive methods are superior to sampling methods in many imbalanced learning domains [25, 26].

The small sample size and disequilibrium of labelled samples make it difficult to detect tool breakage, and auto detection systems rarely exist in the power industry. Therefore, it is worth to develop reliable industrial systems for tool breakage detection. This paper proposes a new method based on an SVM to detect tool breakages and presents an industrial monitoring system for the milling process. This research was conducted on a factory's special rotor slot milling machine, where the milling machine, machine tool, and workpiece material are all large scale and customized. It is difficult to obtain large samples as it is almost impossible to get these items in a laboratory condition. Additionally, the strict safety and quality requirements imposed during production limit the number of tool breakages, so there are far fewer samples of broken tools than normal samples.

Our proposed tool breakage detection system is built based on a cost-sensitive method, which allows us to deal with the imbalanced samples. It has two main phases: the "model establishing" phase, and the "online detection" phase. First, the frequency components of the AE waveform are analysed to screen the tool breakage samples. Second, an SVM-based model is established to reflect the relationship between the AE features and the tool breakages. Third, the performance of the tool breakage detection model is optimized and tested. Our paper provides three main contributions:

1. Because the tool breakages cannot be measured or identified visually during the milling process, we use components of the AE waveform to locate the moments of tool breakages. We then use these moments to retrieve the AE feature samples to establish the breakage detection model.
2. Because there are far fewer broken tool samples than normal samples, we use a cost-sensitive method to improve the performance of SVM on the imbalanced data set.

3.In contrast to previous research, we value the accuracy of the breakage samples and the misclassification rate of the normal samples, respectively. When evaluating the performance of the model, we weigh both rates and then determine the model parameters.

2 Overview of the method

Although the processing technology and the cutting conditions during generator rotor machining process are fixed, insert breakages have inevitably occurred in the past. The objective of our study is to prevent the occurrence of damage to the machined surface and the machine tools by detecting severe breakages. As shown in Fig. 1, the proposed insert breakage detection method has two phases: the model establishing phase and the online detection phase. Since the model establishing phase is an offline process, it is acceptable to have complicated calculation methods. The online detection phase is an industrial application, so that the detection method needs to be easily calculated and have low latency.

In the model establishing phase, we use an AE system to continuously collect raw streaming data and features during the milling process. After the milling process, we use a microscope to measure the breakage value of the inserts. To establish the model, a frequency component analysis method—short-time Fourier transform (STFT)— is applied to screen out the abnormal samples (i.e. the breakage samples) from the normal samples. First, the moments when severe breakages occurred are identified by analysing the frequency components of the AE raw signal. Then, the features of the identified moments are screened out as the abnormal samples. Finally, both the normal and abnormal samples are used to train and optimize an SVM-based breakage detection model.

In the online detection phase, the AE features are extracted and delivered into the breakage detection model in real time during the milling process to decide whether severe breakages have occurred.

3 Experimental setup and instrumentations

3.1 Machining procedure

The experiments were conducted on a factory's customized rotor slot milling machine, as shown in Fig. 2. A piezoelectric

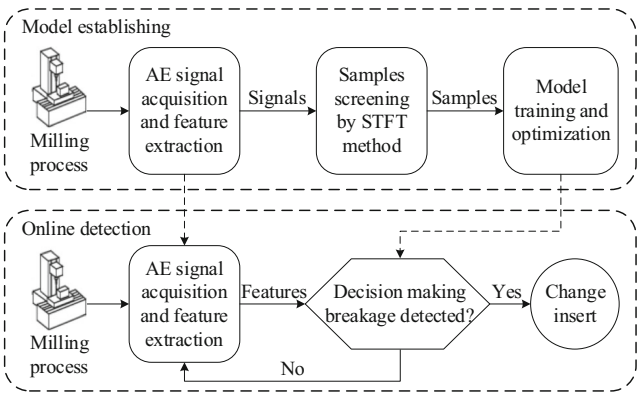

Fig. 1 Schema of the proposed insert breakage detection method

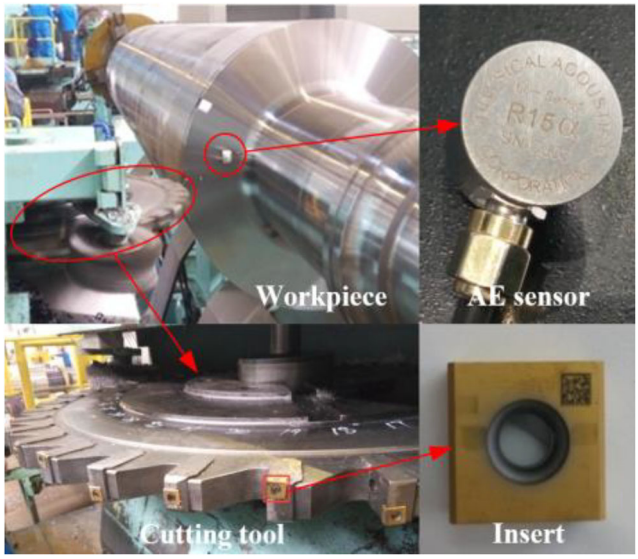

Fig. 2 Experimental setup

AE sensor from the physical acoustics corporation (PAC) was fixed to the surface of the workpiece with a magnetic attraction fixture. A specialized semi-solid acoustic couplant was used to reduce signal transmission loss between the contact surfaces. The next section details the AE signal acquisition setting. The workpiece material is 25Cr2Ni4MoV, a high-strength structural steel. The cutting tool is a W40 disc-type milling cutter, on which 36 SNC55 inserts are mounted as cutting edges. The SNC55 insert is a type of tungsten carbide insert, the parameters of which are shown in Fig. 3. Table 1 shows the experiment conditions.

Five subsequent experiments were conducted under identical experimental conditions except the mechanical properties of the workpiece material. To characterize mechanical performance of the workpiece, tension tests were performed. For each workpiece, six samples from different parts were tested. The averages and standard deviations of yield strength and tensile strength are shown in Table 2.

3.2 AE system

Since the frequency of the AE signal produced in this type of milling is 100–400 kHz [30], the adopted AE sensor is R15α with an operating frequency range of 100–450 kHz, as shown in Fig. 2. A commercial, two-channel AE signal acquisition and digital signal processing system integrated on a full-size PCI card by PAC was used. The system can provide 18-bit A/D conversion, with up to 10 MHz AE data streaming continuous recording on one channel, or 5 MHz on two channels, and a built-in, real-time AE feature extraction. There are two types of real-time extracted AE features: time domain features, which include the rise time (RT), counts (C), amplitude (A), root mean square (RMS), average signal level (ASL), counts to peak (CP), signal strength (SS), and absolute energy (ABE), and frequency domain features, which include the average frequency (AF), reverberation frequency (RF), initiation frequency (IF), and frequency centroid (FC). Figure 4 is a schematic AE signal onto which some of the features have been shown. The calculating formula of the features is detailed in Table 3. The AE signals are sampled at 2 MHz according to the sampling theorem and are processed by AEwin software from PAC. The principal parameters of the recording equipment are detailed in Table 4.

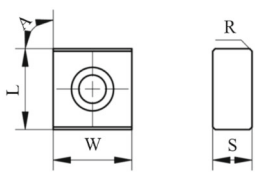

L = W = 15.875 mm, S = 7.94 mm, R = 0.5 mm×45°, A = 90°.

Fig. 3 Shape and dimension of cutting insert. $L = W = 15.875$ mm, $S = 7.94$ mm, $R = 0.5$ mm × 45°, $A = 90°$

The raw AE streaming data, as shown in Fig. 5, is a type of waveform signal. The 12 real-time extracted AE features are a time series signal with time-domain and frequency-domain information. Figure 6 shows the variations of three typical features during one slot milling process. The variation consists of three stages: the start stage, stable cutting stage, and end stage. The start stage and end stage are both unstable transition parts and will be jettisoned when processing the signals. For one slot, 2760 feature samples are extracted during the milling process. We exclude 510 samples corresponding to the start stage and end stage and use the 2250 samples corresponding to the stable cutting stage as the sample to be studied.

3.3 Breakage measurement

We used an optical microscope to measure the breakage values of the inserts. The maximal magnification of the microscope is × 160, and the measurement resolution is 1 μm. There are 4 cutting edges on each SNC55 insert, which are independent from one another. In this experiment, 234 cutting edges were measured. The majority of these cutting edges only had slight breakage, shown in Fig. 7a, which was treated as flank wear. A few cutting edges had severe breakage that far exceeded the normal wear, as shown in Fig. 7b. The acceptable limit of flank wear is 0.6 mm for rough machining [31]. Consequently, the enterprise norm indicates that a cutting edge with more than 1 mm of breakage should be replaced to prevent the occurrence of workpiece damage. There were 17 cutting edges with more than 1 mm of breakage, and these were used as our breakage samples.

Table 1 Experiment conditions

Machine	INGERSOLL rotor slot milling machine
Cutting tool	W40 disc-type milling cutter with 36 SNC55 inserts divided into upper, middle, and lower three places, with a diameter of 1100 mm, and a cutting width of 42.1 mm.
Work material	25Cr2Ni4MoV steel, with a tensile strength of more than 760 MPa, a diameter of 1130 mm, and a length of 6250 mm.
Cutting conditions	Dry cutting, with a spindle speed of 35 rpm, a feed rate of 350 mm/min, and a cutting depth of 50 mm.

4 Signal screening

Since the machine tool is continuously rotating, an insert breakage cannot be identified immediately. We use a time-frequency analysis method to identify the moments of insert breakages. These identified breakage samples, together with the normal samples, are then used to train and optimize the breakage detection model.

The raw AE streaming data, shown in Fig. 5, are a type of waveform signal. Therefore, it cannot be used directly for breakage recognition. The twelve real-time extracted AE features, as previously detailed in Table 2, are time series signals with either time-domain or frequency-domain information. These features have been proved to be related to tool condition [7, 32] and can be used as the input of the learning machine.

Insert breakages cannot be identified by visually inspecting the AE signals (neither the features nor the waveform) or by monitoring the machine tool because it is continuously turning. The frequency components of the AE raw signal vary with the tool condition, and they can be analysed using a time-frequency analysis method [30, 33]. Previous studies have well documented that the STFT method can be used to deal with nonstationary signals and it has been applied to complex signal processing [34, 35]. Frequency components, which are different from the main signal, can be distinctly separated [36]. Furthermore, the STFT method is more suitable than wavelet filters for the analysis of disturbance data, which do not give easy insight in the time behaviour [37]. In view of this, we use the STFT method to locate the moments of insert breakages by analysing the frequency components of the AE raw signal.

The procedure of STFT is to partition a longer temporal signal into shorter segments of equal duration with a window function and to compute the Fourier transform of each shorter segment, respectively. The Fourier spectrum of each shorter segment can then be plotted as a function of time. Assuming an energy-limited signal, $f(t)$ can be decomposed by STFT:

$$(\mathrm{STFT})(f(t)) = \int_{-\infty}^{\infty} f(t)g(t-u)e^{-j\omega t}dt = \langle f(t), \varphi_{u,\omega} \rangle. \quad (1)$$

Here $g(t)$ is a sliding window function (we use the Hamming window in this paper). We can then obtain a localized time–frequency atom φ:

$$\varphi_{u,\omega}(t) = e^{j\omega t}g(t-u). \quad (2)$$

We use a spectrogram, the energy density $|\mathrm{STFT}(f(t))|^2$, to analyse the frequency components. For convenience, the raw signal is divided into parts with equal duration of 10 s. The length of the Hamming window is 256, and the number of overlapped samples is 250. As shown in Fig. 8a, when all machine tool inserts are intact, the spectrogram of the raw AE signal is mainly limited to 50~150 kHz and the energy density in other frequency bands is less than − 100 dB. In the case shown in Fig. 8b, the spectrogram contains not only the 50~150 kHz frequency component but also a short-lived, greater than 200 kHz frequency component. When all factors except for the machine tool condition remain unchanged, we derive the relation between the signal exceptions and insert breakages. From this, we obtain the moments of the insert breakages. We then use these moments to retrieve the AE features corresponding to the insert breakages. Seventeen AE feature samples are screened out, and the number is equal to the number of broken cutting edges.

Unlike breakage samples, normal samples do not need to be screened. The signals of the first slot of the experiment, as shown in Fig. 8a, acquired when all cutting edges are intact, are therefore chosen as the normal samples. As shown in Fig. 6, the normal samples exclude the start and end stages, and only 2250 samples of the stable cutting stage are reserved. The

Table 2 Mechanical properties of the workpiece material

Workpiece no.	1	2	3	4	5
Average of yield strength (MPa)	696.3	697.5	710.8	699.5	702.8
Standard deviation of yield strength (MPa)	7.2	11.1	8.4	19.4	12.5
Average of tensile strength (MPa)	799.3	813.3	825.8	807.8	808.3
Standard deviation of tensile strength (MPa)	3.7	7.5	5.3	10.6	7.5

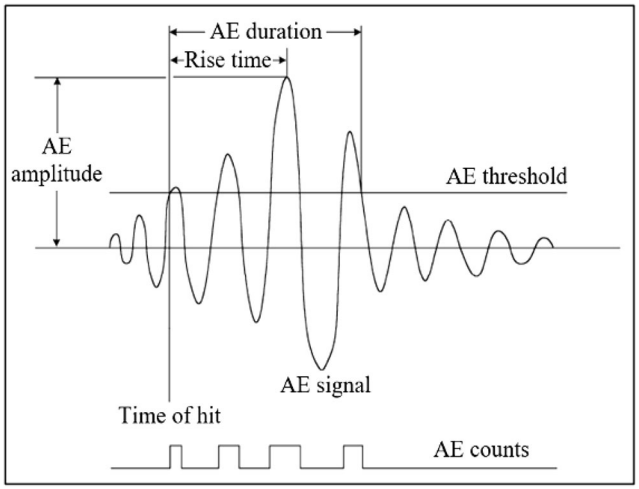

Fig. 4 Schematic diagram of the AE signal

17 abnormal samples and 2250 normal samples are used to form the learning sample set.

5 Detection of insert breakage

5.1 Breakage detection model

The detection of severe breakages is a very sophisticated problem that involves the establishment of a detection model and optimization of the model's performance. The screened sample set can be expressed as

$$X = \{(x_i, y_i), i = 1, 2, \cdots, n\}. \tag{3}$$

Table 4 Parameters of the recording equipment

Threshold	45 dB
Pre-amplifier	20 dB
Analogue filter	100–400 kHz
Digital filter	Disabled
Maximum duration	100 ms
Streaming record length	10 s
RMS/ASL time constant	500 ms

Here $x_i = (RT_i, C_i, A_i, AF_i, RMS_i, ASL_i, CP_i, RF_i, IF_i, SS_i, ABE_i, FC_i)^T$ is the signal feature vector of the ith sample, $y_i \in \{1, -1\}$ is the class label of the ith sample, and n is the size of the dataset.

The large differences in the scales and magnitudes of the twelve features can impact the accuracy of the model. Therefore, it is critical to standardize the features to enhance their comparability. In this paper, we employ dispersion to standardize the features. Taking the RT for example, the calculation formula is

$$RT_i^* = \frac{RT_i - RT_{\min}}{RT_{\max} - RT_{\min}} i = 1, 2, \cdots, n. \tag{4}$$

The standardized features, with a distribution range of [0, 1], form the input matrix of the breakage detection model:

$$X^* = \left(x_1^*, x_2^*, \ldots, x_n^*\right) = \begin{pmatrix} RT_1^* & RT_2^* & \cdots & RT_n^* \\ C_1^* & C_2^* & \cdots & C_n^* \\ \vdots & \vdots & \ddots & \vdots \\ FC_1^* & FC_2^* & \cdots & FC_n^* \end{pmatrix}. \tag{5}$$

Table 3 Definitions of AE features

Features	Abbreviation	Definition
Rise time	RT	The time between an AE hit starts, and it reaches the peak amplitude.
Counts	C	The number of AE signal excursions over the AE threshold.
Amplitude	A	$A = 120 \log V_{\max} - P$ (dB), where P is preamplification gaining.
Root mean square	RMS	$\mathrm{RMS} = \sqrt{\frac{1}{N}\sum_{i=1}^{N} V_i^2}$.
Average signal level	ASL	$\mathrm{ASL} = 120 \log \overline{V}$ (dB).
Counts to peak	CP	The number of C between its start and peak amplitude.
Signal strength	SS	$\mathrm{SS} = \frac{1}{2f_s}\sum_{i=1}^{N-1}(V_i + V_{i+1})$, where f_s is sample rate.
Absolute energy	ABE	$\mathrm{ABE} = \frac{1}{10\mathrm{k}\Omega}\sum_{i=1}^{N} V_i^2$, where 10kΩ is the reference resistance of the recording equipment.
Average Frequency	AF	$AF = C/HT$, where HT is the duration of an AE hit.
Reverberation Frequency	RF	$RF = \frac{C - CP}{HT - RT}$.
Initiation frequency	IF	$IF = CP/RT$.
Frequency centroid	FC	$FC = \frac{\sum f \cdot \widetilde{V}}{\sum \widetilde{V}}$ is calculated from fast Fourier transform (FFT), where $\widetilde{V}$ is the magnitude of FFT element and f is corresponding frequency.

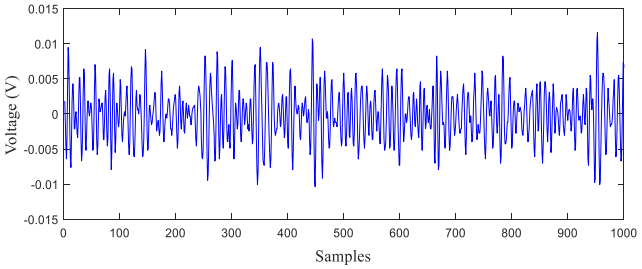

Fig. 5 AE streaming data

The output values of the breakage detection model are set to 1" and "−1" for the abnormal and normal samples, respectively. The output vector for training and detection is

$$Y = (y_1, y_2, \cdots, y_n)^T. \tag{6}$$

The standard SVM is proposed for binary classification problems. The fundamental of the SVM is to maximize the certainty factor by finding a separating hyperplane, which maximizes the margin between two classes.

Assume that the input matrix and their labels are $\{x_i^*, y_i\}$, $i = 1, 2, \cdots, n$, and $y_i \in \{1, -1\}$. The modelling process of the SVM can be converted into solving this dual problem:

$$\min_{\alpha} \quad \frac{1}{2}\sum_{i=1}^{n}\sum_{j=1}^{n}\alpha_i\alpha_j y_i y_j K(x_i, x_j) - \sum_{i=1}^{n}\alpha_i \tag{7}$$
$$s.t. \quad 0 \le \alpha_i \le C, \quad i = 1, 2, \cdots, n \qquad \sum_{i=1}^{n}\alpha_i y_i = 0.$$

Here, α_i, $i = 1, 2, \cdots, n$ are the parameters to be solved, C is the penalty factor corresponding to the trade-off between the empirical error and the regularized term, and $K(x_i, x_j) = \langle \Phi(x_i) \cdot \Phi(x_j) \rangle$ is the kernel function, which can ensure the model to be exempt from "dimension disaster" in high-dimensional feature space. In this paper, we employ radial basis function:

$$K(x_i, x_j) = \exp\left(-\gamma \left\| x_i - x_j \right\|^2\right). \tag{8}$$

This is a convexity quadratic programming problem that has a unique solution. The solving process and solution are relevant only to the input matrix.

Our acquired data set contains 17 breakage samples and 2250 normal samples. A usual classifier that classifies all the samples into the majority can reach an accuracy of 99.3%. However, the minority samples, which are our focus, would all be misclassified. Therefore, to improve the detection rate of the breakage, we adopt a type of cost-sensitive SVM. This is implemented by introducing different penalty factors, C_1 and C_{-1}, for the minority samples and majority samples during training, and the standard SVM problem is transformed into

$$\min_{\alpha} \quad \frac{1}{2}\sum_{i=1}^{n}\sum_{j=1}^{n}\alpha_i\alpha_j y_i y_j K(x_i, x_j) - \sum_{i=1}^{n}\alpha_i \tag{9}$$
$$s.t. \quad 0 \le \alpha_i \le C_i, \quad i = 1, 2, \cdots, n \qquad \sum_{i=1}^{n}\alpha_i y_i = 0.$$

Here, $C_i = \{ C_1 \quad i \in \{i | y_i = 1\} \; C_{-1} i \in \{i | y_i = -1\}$. The introduction of different penalty factors enables the learning machine to treat the minority and the majority, respectively, namely, the cost of misclassification of abnormal samples is much higher than the normal ones. The higher misclassification cost of the abnormal samples can contribute to the lower misclassification rate of the abnormal samples; consequently, the breakage detection performance of the model can be improved. Thereafter, the classification results can be calculated through this optimal function:

$$f(x) = \mathrm{sgn}\left\{\sum_{i=1}^{n}\alpha_i^* y_i K(x_i, x_{test}) + b_0\right\}. \tag{10}$$

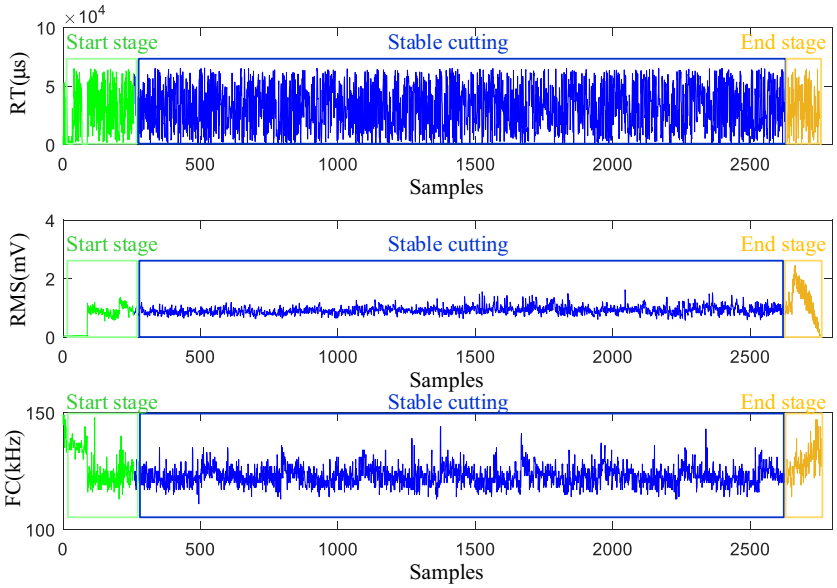

Fig. 6 Variations of some features

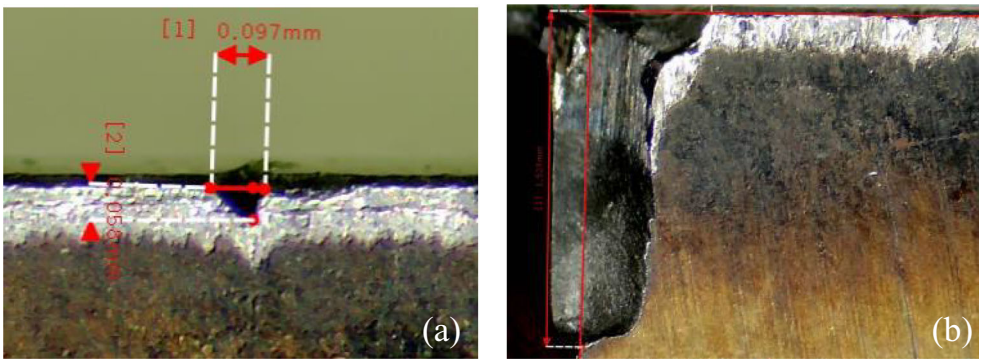

Fig. 7 **a** Slight breakage of majority. **b** Severe breakage of minority

Here, x_{test} is the sample to be classified, and b_0 is the classification margin calculated using any one of the support vectors.

When performing prediction we wish not only to obtain the predicted label but also gain an uncertainty, or a probability of the respective label. This uncertainty or probability gives some kind of confidence of the prediction. However, SVM produces an uncalibrated value that is not a probability. So that we use Platt's probabilistic outputs [38], which train an additional sigmoid function to transform the original SVM outputs into probabilities. It is a posterior probability approximated by a sigmoid function:

$$\Pr(y=1|x)\approx P_{A,B}(f')\equiv\frac{1}{1+\exp(Af'+B)}, \tag{11}$$

where $f'=\sum_{i=1}^{n}\alpha_i^* y_i K(x_i, x_{test})+b_0$ is the unthresholded output of the SVM. The best parameter setting $z^*=(A^*,B^*)$ is obtained by solving this regularized maximum likelihood problem (with N_+ of the y_i positive, and N_- negative):

$$\min_{z=(A,B)} F(z)=-\sum_{i=1}^{n}(t_i\log(p_i)+(1-t_i)\log(1-p_i)), \tag{12}$$

$$\text{for } p_i=P_{A,B}(f_i'),\text{ and } t_i=\begin{cases}\frac{N_++1}{N_++2} & \text{if } y_i=+1\\ \frac{1}{N_-+2} & \text{if } y_i=-1\end{cases}, \quad i=1,\cdots,n..$$

The optimization algorithm of (12) is Newton's method with backtracking [39].

5.2 Model training and optimization

The performance of a method is generally evaluated by its accuracy. In this paper, a total of 17 abnormal samples and 2250 normal samples are screened out for the model training and testing. Assumed the model classifies all the samples into the majority, it can achieve an accuracy of 99.3%; however, it would also misclassify all of the breakage samples. We therefore use the true positive rate (TPR) and the false positive rate (FPR) to evaluate the performance of the model. *TPR* and *FPR* can be calculated using

$$TPR=\frac{TP}{TP+FN}, \tag{13}$$

$$FPR=\frac{FP}{FP+TN}. \tag{14}$$

Here, *TP* is the number of correctly classified majority (the normal data set) samples with label "−1," *FN* is the number of misclassified minority (the breakage data set) samples with label "1," *FP* is the number of misclassified majority samples, and *TN* is the number of correctly classified majority samples.

For the 2250 normal samples, we use the first 2000 samples as the training dataset and use the remaining 250 samples as the testing dataset to validate the model. As a result, the training and testing data set of the majority have enough samples. In contrast, the minority data set is made up of only 17

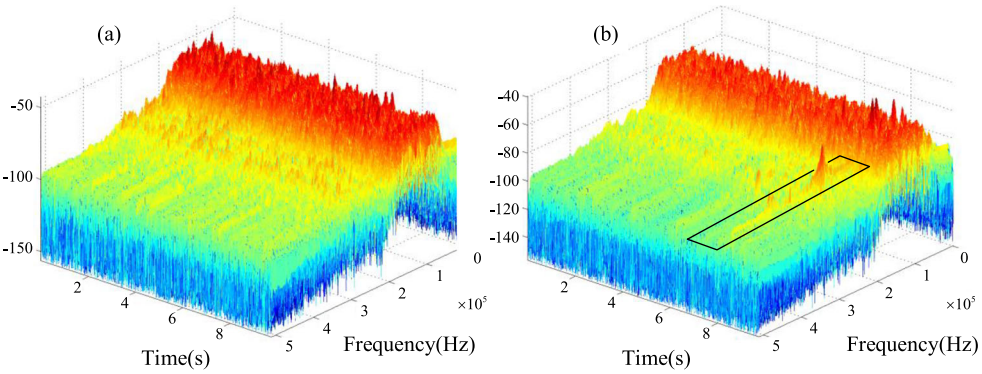

Fig. 8 **a** STFT of the normal AE signal. **b** STFT of the abnormal AE signal

Table 5 Sampling results for validation

Sample no.	Sampling results						
1	1	2	3	6	8	11	17
2	1	2	3	8	10	13	17
3	2	3	13	14	15	16	17
4	1	3	5	7	8	9	13
5	4	5	9	10	11	13	16
6	2	4	10	11	12	14	17
7	1	2	4	9	14	16	17
8	1	3	5	8	10	14	15
9	1	2	3	8	9	10	15
10	1	5	7	8	13	16	17

samples, where each sample has the potential to be different because of the random manner in which breakages occur. To eliminate the adverse impact of individuality of minority sample on model validation, we select samples for validation ten times using the random sampling method. The minority samples are labelled from 1 to 17 at each validation, where 7 of them are selected randomly as the testing dataset and the remaining 10 are used as the training dataset. The random sampling results are presented in Table 5. While optimizing the breakage detection model, the model is trained using the training data, and tested with the testing data together with training data ten times, with an average *FPR* and *TPR*, then calculated to evaluate the model.

The performance of the model depends on the choice of C_i in (9) and γ in (8). For the pairing of C and γ, the grid search method is applied for model optimization:

(1) Search well performance range of γ and C_i. Set $C_1 = C_{-1} = C = 2^{\alpha}$, $\gamma = 2^{\beta}$, then let $\alpha, \beta = -20:2:20$, change by exponential mean to perform successive grid search. For every combination of γ and C, the model is trained and tested using the ten sets of sample data, and the average *FPR* and *TPR* are calculated to evaluate the model.

(2) Shrink the scope of γ and C. In the first step, rough variations of *FPR* and *TPR* with γ and C are gained. Then, shrink the scope and step size of α to $\alpha = 0:0.5:20$, and shrink the scope and step size of β to $\beta = -5:0.25:5$. The optimal combination of these is determined to be $\gamma = 2^{-3.25}$, $C \geq 2^{10}$.

(3) Search C_1 and C_{-1} using the grid search method. On the basis of the last step, set γ to a optimal value$2^{-3.25}$ and let C_1 and C_{-1} change by exponential mean. In the same way, the model is trained and tested with ten sets of sample data and the average *FPR* and *TPR* are calculated to evaluate the model. Grid images of the average *TPR* and *FPR* are drawn, as shown in Fig. 9. At the top left of line transition 1, the average *TPR* can reach 100%; however, the *FPR* is higher than 15.57%, which means that too many negative samples are misclassified as positive. Between the line transition 1 and line transition 2, the average *TPR* is in the range of 88.82~100%, and the average *FPR* is between 0.21 and 15.57%. The average *TPR* reduces when the average *FPR* reduces. At the bottom right of line transition 2, the average *TPR* stabilizes at around 91.18%, and the average *FPR* stabilizes at around 0.03%. The circled area is the boundary region, where the average *TPR* declines sharply together with the average *FPR*.

5.3 Breakage detection results

Ultimately, the optimal combination of the three parameters, γ, C_1, and C_{-1}, is determined by analysing the variation of the average *FPR* and *TPR* with the parameters. It is difficult for the average *TPR* and *FPR* to attain superiority simultaneously. Consequently, we weigh the advantages and disadvantages of their influence on breakage detection.

Table 6 shows the optimization results of two parameter settings. Here, *TPR* and *FPR* are the indicators mentioned above, and N_1 is the number of misclassified

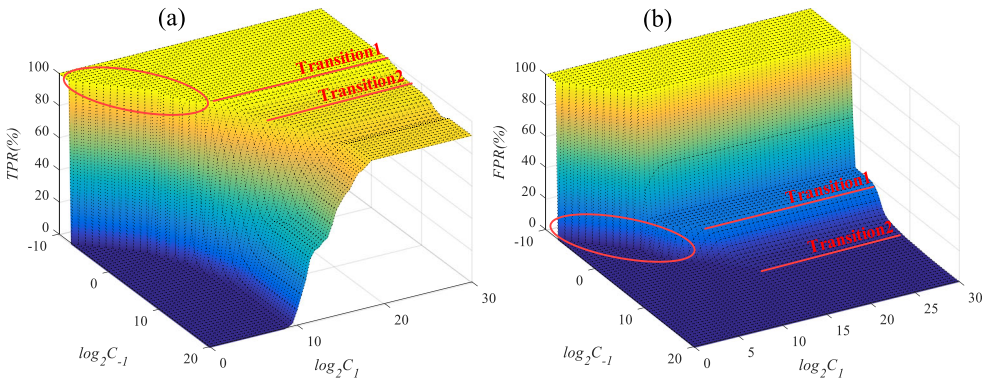

Fig. 9 **a** Average *TPR* of the model. **b** Average *FPR* of the model

Table 6 Optimization results

Parameters combination	*TPR*	*FPR*	N_1	N_{-1}	*E*	P_1	P_{-1}
$\gamma = 2^{-3.25}$, $C_{-1} = 2^{16.5}$, $C_1 = 2^{18}$	91.18%	0.03%	1.5	0.6	0.03%	0.667	0.999
$\gamma = 2^{-3.25}$, $C_{-1} = 2^{11}$, $C_1 = 2^{15.5}$	93.53%	0.64%	1.1	14.5	0.27%	0.672	0.978

abnormal samples, N_{-1} is the number of misclassified normal samples, E is the error obtained after training, P_1 is the mean classification probability of test abnormal samples, and P_{-1} is the mean classification probability of test normal samples. It should be noted that these indicators are all the average of ten test runs.

In our opinion, the optimal parameter values are $\gamma = 2^{-3.25}$, $C_{-1} = 2^{16.5}$, and $C_1 = 2^{18}$ when the average $TPR = 91.18\%$ and $FPR = 0.03\%$. Under this condition, the mean of misclassified abnormal samples is 1.5, and the mean of misclassified normal samples is 0.6. In another case, when the average $TPR = 93.53\%$ and $FPR = 0.64\%$, the values of the parameters are $\gamma = 2^{-3.25}$, $C_{-1} = 2^{11}$, and $C_1 = 2^{15.5}$. Under this condition, the mean of misclassified abnormal samples is 1.1 and the mean of misclassified normal samples is 14.5. Here, the number of misclassified abnormal samples decreases few at the cost of much higher misclassification of the normal samples. Under the first condition, the error obtained after training is even smaller although it is quite small in both cases. The mean classification probability of test normal samples approaches to 1, indicating it is almost impossible to misclassify normal samples. The mean classification probability of test abnormal samples is near to that in another case. Therefore, our suggested optimal parameter values are shown to be generally balanced and well performing.

6 Conclusions

In this paper, we propose a tool breakage detection method based on short-time Fourier transform (STFT) and a support vector machine (SVM) to detect catastrophic tool failure. Acoustic emission (AE) streaming data and twelve real-time extracted features of a milling process are obtained from a factory's special rotor slot milling machine. We use an STFT method to analyse the frequency components of the AE streaming data. Seventeen moments of tool breakages are located, and the corresponding AE feature samples are screened out as the abnormal data set. We then establish a cost-sensitive breakage detection model and optimize the parameters using a grid search method. To evaluate the performance of our model, we consider both the true positive rate (TPR) and the false positive rate (FPR). We determine optimal parameter values, which are shown to be generally balanced and well performing. As a result, our model achieves an average $TPR = 91.18\%$ and $FPR = 0.03\%$, which demonstrates the validity and practicability of our proposed method.

Our method consists of two phases: the model establishing (offline) phase and the online phase. The complicated computational procedures are completed in the model establishing phase. In the online phase, the insert breakages are detected in real time using real-time extracted AE features and a pretrained model. Our method can promptly detect almost all severe breakages, which prevents damage to the product's machined surface and the machine tools. The proposed method guarantees the quality of the machined surface and the efficiency of the machining process.

There are some limitations in our study. First, subject to false detection rate, the undetected rate of breakage samples is still a little high. Second, the experiments were carried out under particular conditions, and if the cutting conditions or the properties of the material change, the detection model will need to be retrained. Considering these limitations, Future studies will focus on (a) designing better detection methods to further improve detection accuracy and false detection rate and (b) developing methods that are easily applied to different milling conditions.

Funding information This work has been supported by the National Natural Science Foundation of China (Grant No. 51435009) and Science and Technology Commission of Shanghai Municipality (No. 19511105302).

References

1. Neslušan M, Mičieta B, Mičietová A, Čilliková M, Mrkvica I (2015) Detection of tool breakage during hard turning through acoustic emission at low removal rates. Measurement 70:1–13. https://doi.org/10.1016/j.measurement.2015.03.035
2. Corne R, Nath C, El Mansori M, Kurfess TJ (2017) Study of spindle power data with neural network for predicting real-time tool wear/breakage during inconel drilling. J Manuf Syst 43:287–295
3. Wong SY, Chuah JH, Yap HJ (2020) Technical data-driven tool condition monitoring challenges for CNC milling: a review. Int J Adv Manuf Technol
4. Zhou YQ, Xue W (2018) Review of tool condition monitoring methods in milling processes. Int J Adv Manuf Technol 96(5-8): 2509–2523
5. Pai PS, Rao PKR (2002) Acoustic emission analysis for tool wear monitoring in face milling. Int J Prod Res 40(5):1081–1093

6. Hase A, Wada M, Koga T, Mishina H (2014) The relationship between acoustic emission signals and cutting phenomena in turning process. Int J Adv Manuf Technol 70(5-8):947–955
7. Liu YC, Hu XF, Yan S, Sun SX (2017) Tool condition monitoring and degradation estimation in rotor slot machining process. Int J Adv Manuf Technol 91(1-4):39–48
8. Teti R, Jemielniak K, O'Donnell G, Dornfeld D (2010) Advanced monitoring of machining operations. CIRP Ann Manuf Technol 59(2):717–739
9. Yesilyurt I, Ozturk H (2007) Tool condition monitoring in milling using vibration analysis. Int J Prod Res 45(4):1013–1028
10. Liu TI, Song SD, Liu G, Wu Z (2013) Online monitoring and measurements of tool wear for precision turning of stainless steel parts. Int J Adv Manuf Technol 65(9-12):1397–1407
11. Denkena B, Tonshoff HK, Li X, Imiela J, Lapp C (2004) Analysis and control/monitoring of the direct linear drive in end milling. Int J Prod Res 42(24):5149–5166
12. Reñones A, Rodríguez J, de Miguel LJ (2009) Industrial application of a multitooth tool breakage detection system using spindle motor electrical power consumption. Int J Adv Manuf Technol 46(5-8): 517–528. https://doi.org/10.1007/s00170-009-2119-3
13. Lauro CH, Brandão LC, Baldo D, Reis RA, Davim JP (2014) Monitoring and processing signal applied in machining processes – A review. Measurement 58:73–86. https://doi.org/10.1016/j.measurement.2014.08.035
14. Rmili W, Ouahabi A, Serra R, Leroy R (2016) An automatic system based on vibratory analysis for cutting tool wear monitoring. Measurement 77:117–123. https://doi.org/10.1016/j.measurement.2015.09.010
15. Rehorn AG, Jiang J, Orban PE (2005) State-of-the-art methods and results in tool condition monitoring: a review. Int J Adv Manuf Technol 26(7-8):693–710
16. Ren Q, Balazinski M, Baron L, Jemielniak K, Botez R, Achiche S (2014) Type-2 fuzzy tool condition monitoring system based on acoustic emission in micromilling. Inf Sci 255:121–134
17. Xu GD, Zhou HC, Chen JH (2018) CNC internal data based incremental cost-sensitive support vector machine method for tool breakage monitoring in end milling. Eng Appl Artif Intell 74:90–103
18. Cho S, Asfour S, Onar A, Kaundinya N (2005) Tool breakage detection using support vector machine learning in a milling process. Int J Mach Tools Manuf 45(3):241–249
19. Hsueh YW, Yang CY (2008) Prediction of tool breakage in face milling using support vector machine. Int J Adv Manuf Technol 37(9-10):872–880. https://doi.org/10.1007/s00170-007-1034-8
20. Kuljanic E, Totis G, Sortino M (2009) Development of an intelligent multisensor chatter detection system in milling. Mech Syst Signal Process 23(5):1704–1718
21. Tobon-Mejia DA, Medjaher K, Zerhouni N (2012) CNC machine tool's wear diagnostic and prognostic by using dynamic Bayesian networks. Mech Syst Signal Process 28:167–182
22. Geramifard O, Xu JX, Zhou JH, Li X (2012) A physically segmented hidden Markov model approach for continuous tool condition monitoring: diagnostics and prognostics. IEEE Trans Ind Inf 8(4): 964–973
23. Mountrakis G, Im J, Ogole C (2011) Support vector machines in remote sensing: a review. ISPRS J Photogramm Remote Sens 66(3):247–259
24. Pal M, Foody GM (2010) Feature selection for classification of hyperspectral data by SVM. IEEE Trans Geosci Remote Sens 48(5):2297–2307
25. Haibo H, Garcia EA (2009) Learning from imbalanced data. IEEE Trans Knowl Data Eng 21(9):1263–1284. https://doi.org/10.1109/tkde.2008.239
26. Guo HX, Li YJ, Shang J, Gu MY, Huang YY, Bing G (2017) Learning from class-imbalanced data: review of methods and applications. Expert Syst Appl 73:220–239
27. Bach M, Werner A, Zywiec J, Pluskiewicz W (2017) The study of under- and over-sampling methods' utility in analysis of highly imbalanced data on osteoporosis. Inf Sci 384:174–190
28. Ting KM (2002) An instance-weighting method to induce cost-sensitive trees. IEEE Trans Knowl Data Eng 14(3):659–665
29. Yan JH, Han SQ (2018) Classifying imbalanced data sets by a novel RE-sample and cost-sensitive stacked generalization method. Math Prob Eng
30. Marinescu I, Axinte DA (2008) A critical analysis of effectiveness of acoustic emission signals to detect tool and workpiece malfunctions in milling operations. Int J Mach Tools Manuf 48(10):1148–1160
31. Lim G (1995) Tool-wear monitoring in machine turning. J Mater Process Technol 51(1-4):25–36
32. Dimla DE (2000) Sensor signals for tool-wear monitoring in metal cutting operations—a review of methods. Int J Mach Tools Manuf 40(8):1073–1098
33. Chen XZ, Li BZ (2007) Acoustic emission method for tool condition monitoring based on wavelet analysis. Int J Adv Manuf Technol 33(9-10):968–976
34. Li XL (2002) A brief review: acoustic emission method for tool wear monitoring during turning. Int J Mach Tools Manuf 42(2): 157–165
35. Zhu KP, San WY, Soon HG (2009) Wavelet analysis of sensor signals for tool condition monitoring: a review and some new results. Int J Mach Tools Manuf 49(7-8):537–553
36. Kuang WT, Morris AS (2002) Using short-time Fourier transform and wavelet packet filter banks for improved frequency measurement in a Doppler robot tracking system. IEEE Trans Instrum Meas 51(3):440–444
37. Gu YH, Bollen MHJ (2000) Time-frequency and time-scale domain analysis of voltage disturbances. IEEE Trans Power Deliv 15(4):1279–1284
38. Platt J (1999) Probabilistic outputs for support vector machines and comparisons to regularized likelihood methods. Adv Large Margin Classifiers 10(3):61–74
39. Lin HT, Lin CJ, Weng RC (2007) A note on Platt's probabilistic outputs for support vector machines. Mach Learn 68(3):267–276